

Doc-Start

Structural bioinformatics

Sequence-structure relations of biopolymers

Christopher Barrett¹, Fenix W. Huang¹ and Christian M. Reidys^{1*}¹Virginia Bioinformatics Institute, 1015 Life Sciences Circle, Blacksburg, VA, USA

*To whom correspondence should be addressed.

Associate Editor: XXXXXXXX

Received on XXXXX; revised on XXXXX; accepted on XXXXX

Abstract

Motivation: DNA data is transcribed into single-stranded RNA, which folds into specific molecular structures. In this paper we pose the question to what extent sequence- and structure-information correlate. We view this correlation as structural semantics of sequence data that allows for a different interpretation than conventional sequence alignment. Structural semantics could enable us to identify more general embedded “patterns” in DNA and RNA sequences.

Results: We compute the partition function of sequences with respect to a fixed structure and connect this computation to the mutual information of a sequence-structure pair for RNA secondary structures. We present a Boltzmann sampler and obtain the a priori probability of specific sequence patterns. We present a detailed analysis for the three PDB-structures, 2JXV (hairpin), 2N3R (3-branch multi-loop) and 1EHZ (tRNA). We localize specific sequence patterns, contrast the energy spectrum of the Boltzmann sampled sequences versus those sequences that refold into the same structure and derive a criterion to identify native structures. We illustrate that there are multiple sequences in the partition function of a fixed structure, each having nearly the same mutual information, that are nevertheless poorly aligned. This indicates the possibility of the existence of relevant patterns embedded in the sequences that are not discoverable using alignments.

Availability: The source code is freely available at <http://staff.vbi.vt.edu/fenixh/Sampler.zip>

Contact: duckcr@vbi.vt.edu

Supplementary information: Supplementary material containing additional data tables are available at *Bioinformatics* online.

1 Introduction

2015 is the 25th year of the human genome project. A recent signature publication (The 1000 Genomes Project Consortium, 2015) is a comprehensive sequence alignment-based analysis of whole genome nucleotide sequence variation across global human populations. Notwithstanding the importance of this achievement, there is the possibility of information encoded as patterns in the genome that current methods cannot discover.

In this paper we study the information transfer from RNA sequences to RNA structures. This question is central to the processing of DNA data, specifically the role of DNA nucleotide sequences being transcribed into RNA, stabilized by molecular folding. In a plethora of interactions it is this specific configuration and not the particular sequence of nucleotides

sequences in the partition function of a fixed structure, each having nearly the same mutual information with respect to the latter, that are nevertheless poorly aligned. This indicates the possibility of the existence of relevant patterns embedded in the sequences that are not discoverable using alignments.

RNA, unlike DNA, is almost always single-stranded¹ and all RNA is folded. Here we only consider single-stranded RNA. An RNA strand has a backbone made of alternating sugar (ribose) and phosphate groups. Attached to each sugar is one of four bases—adenine (A), uracil (U), cytosine (C), or guanine (G). There are various types of RNA: messenger RNA (mRNA), ribosomal RNA (rRNA), transfer RNA (tRNA) and many others. Recent transcriptomic and bioinformatic studies suggest the existence of numerous of so called non coding RNA, ncRNAs, that is RNA that does not translate into a protein (Eddy, 2001; Cheng *et al.*, 2005).

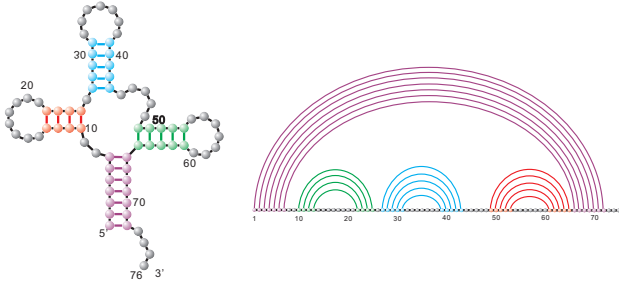


Fig. 1. tRNA: its secondary structure and its diagram presentation.

RNA realizes folded molecular conformations consistent with the Watson-Crick base as well as the wobble base pairs. In the following we consider RNA secondary structures, presented as diagrams obtained by drawing the sequence in a straight line and placing all Watson-Crick and Wobble base pairs as arcs in the upper half-plane, without any crossing arcs, see Fig. 1.

DNA information processing refers to replication, transcription and translation. Additionally, RNA information processing includes replication (Koonin *et al.*, 1989), reverse transcription (from RNA to DNA in e.g. retroviruses) (Temin and Mizutani, 1970) and a direct translation from DNA to protein² (McCarthy and Holland, 1965; Uzawa *et al.*, 2002).

In the following we offer an alternative view of DNA-RNA information processing. We focus on the information transfer from DNA/RNA sequences to the folded RNA (after transcription). We speculate that the sequential DNA information may transcribe into single-stranded RNA in order to allow subsequent biological processes to interpret DNA data.

DNA data are viewed as sequences of nucleotides. We currently use sequence alignment tools as a means of arranging the sequences of DNA, RNA, or proteins to identify regions of similarity that may be a consequence of functional, structural, or evolutionary relationships between the sequences (Mount, 2004). Here we suggest that the transcription into RNA with the implied self-folding is a way of lifting DNA information to a new and different level: RNA structures provide sequence semantics.

In order to study this idea we consider the folding of RNA sequences into minimum free energy (mfe) secondary structures (Waterman, 1978). Pioneered by Waterman more than three decades ago (Smith and Waterman, 1978) and subsequently studied by Schuster *et al.* (Schuster *et al.*, 1994) in the context of the RNA toy world (Schuster, 1997) there is detailed information about this folding. In particular we have fairly accurate energy values for computing loop-based mfe (Mathews *et al.*, 2004) that are employed by the folding algorithms (Zuker and Stiegler, 1981; Hofacker *et al.*, 1994). More work has been done on loop-energy models in (Mathews, 2004; Do *et al.*, 2006). We plan on a more detailed analysis of the framework proposed here in the context of the MC-model (Parisien and Major, 2008).

In (McCaskill, 1990) McCaskill observed that the dynamic programming routines folding mfe structures (McCaskill, 1990) allows one to compute the partition function of all possible structures for a given sequence. The partition function is tantamount to computing the probability space of structures that a fixed sequence is compatible with. Predictions such as base pairing probabilities are obtained in (Hofacker *et al.*, 1994; Hofacker, 2003) and are parallelized in

valid sampling of secondary structures in the Boltzmann ensemble and calculates the sampling statistics of structural features.

In view of the above we are led to consider the “dual” of McCaskill’s partition function, i.e. the partition function of all sequences that are compatible with a fixed structure. More generally we consider the pairing

$$\varepsilon: \mathcal{Q}_4^n \times \mathcal{S}_n \longrightarrow \mathbb{R}, \quad (1)$$

where \mathcal{Q}_4^n and \mathcal{S}_n denote the space of sequences, σ , and the space of secondary structures, S , respectively and $\varepsilon(\sigma, S) = e^{-\frac{\eta(\sigma, S)}{kT}}$ and $\eta(\sigma, S)$ are discussed in Section 2.2.

We show in Section 3 how ε allows us to capture the mutual information between sequences and structures, where the mutual information between the sets X and Y is given by

$$\sum_{x \in X, y \in Y} I(x, y) = \sum_{x \in X, y \in Y} \mathbb{P}(x, y) \log \left(\frac{\mathbb{P}(x, y)}{\mathbb{P}(x)\mathbb{P}(y)} \right)$$

and $\mathbb{P}(x, y)$ denotes the joint probability distribution.

In addition, ε allows us to express folding by considering

$$\{S \mid \varepsilon(\sigma, S) = \min \varepsilon(\sigma, \mathcal{S}_n)\}$$

and inverse folding as to compute $\{\sigma \mid \varepsilon(\sigma, S) = \min \varepsilon(\sigma, \mathcal{S}_n)\}$, for fixed S . Accordingly, the dual to folding is tantamount to computing for fixed S

$$\{\sigma \mid \varepsilon(\sigma, S) = \min \varepsilon(\mathcal{Q}_4^n, S)\}.$$

This has direct implications to the “inverse” folding of structures. Inverse folding is by construction about the sequence constraints induced by a fixed structure while avoiding competing configurations. Point in case: it has been observed in (Busch and Backofen, 2006) that starting with a sequence that is mfe w.r.t. to a fixed structure, without necessarily folding into it, constitutes a significantly better initialization than starting with a random sequence.

The paper is organized as follows: we first recall in Section 2.2 the concept of topological RNA structures since this allows us to connect the loop based energy to topological boundary components. This in turn facilitates (Sections 2.3 and 2.4) the derivation of the partition function and Boltzmann sampling. In Section 2.2 we discuss topology and energy, detailing all loop-types and in Sections 2.3 and 2.4 we compute $Q(S)$, Boltzmann sampling and the a priori probability of sequence patterns.

2 Method

2.1 Topological model of RNA structures

RNA structures can be represented as diagrams where we consider the labels of the sequence to be placed on the x -axis and the Watson-Crick and Wobble base pairs drawn as arcs in the upper half plane see Fig. 2 (A). That is, we have a vertex-labeled graph whose vertices are drawn on a horizontal line labeled by $[n] = \{1, 2, \dots, n\}$, presenting the nucleotides of the RNA sequence and the linear order of the vertices from left to right indicates the direction of the backbone from 5’-end to 3’-end. Furthermore each vertex can be paired with at most one other vertex by an arc drawn in the upper half-plane. Such an arc, (i, j) , represents the base pair between the i th and j th nucleotide³.

An RNA structure is called pseudoknot-free or secondary structure,

implies that the diagram contains only noncrossing arcs (Fig. 2 (A)). We shall equip any structure over a sequence of length n with the “rainbow” arc, $(0, n + 1)$, adding the “virtual” nucleotides $0, n + 1$, see Fig. 2 (A).

The topological model for RNA structures is due to the work in (Penner and Waterman, 1993; Penner, 2004) and the classification and expansion of RNA structures including pseudoknots in terms of the topological genus of an associated fatgraph has been studied by means of matrix theory in (Orland and Zee, 2002; Bon *et al.*, 2008). The equation to compute the genus of a fatgraph is classical going back to (Euler, 1752) and was first applied in the context representing RNA structures by (Orland and Zee, 2002) and (Bon *et al.*, 2008). Later in (Andersen *et al.*, 2012), topological RNA structures of higher genus were studied and brought into context with Moduli spaces in (Penner, 2004). In (Reidys *et al.*, 2011) a loop-based folding algorithm of topological RNA structures is given.

In essence the idea is to pass from diagrams to fatgraphs (Penner, 1988; Loebl and Moffatt, 2008; Penner *et al.*, 2010), by “thickening” the edges of the diagram into untwisted ribbons, and inflating each vertex to a disc, Fig. 2 (B). This immediately becomes clear when trying to draw a diagram on a surface since an order of the edges around a fixed vertex has to be chosen.

The inflation replaces the set of edges by ribbons, represented by two half edges and vertices by a sequence of half edges. If we rotate counterclockwise around any vertex any ribbon is traversed complementarily, that is its sides are traversed in opposite directions. The two half edges labeling the ribbon are obtained as follows: one cuts the two respective sides in half and marks the half which is traversed towards its incident vertex.

A fatgraph, \mathbb{D} , is thus a “drawing” on an orientable surface $X_{\mathbb{D}}$, \mathbb{D} , i.e. a 2-dimensional cell-complex over its geometric realization, $X_{\mathbb{D}}$, realized by identifying all pairs of complementary edges. As a drawing on $X_{\mathbb{D}}$ the complement of \mathbb{D} is a disjoint union of discs.

Topological invariants such as the Euler characteristic χ and topological genus of the surface \mathbb{D} are given by

$$\chi(\mathbb{D}) = v - e + r, \quad g(\mathbb{D}) = 1 - \frac{1}{2}\chi(\mathbb{D}),$$

where v , e and r denote the number of discs, ribbons and boundary components in \mathbb{D} (Massey, 1967). The equivalence of simplicial and singular homology (Hatcher, 2002) implies that these combinatorial invariants are in fact invariants of $X_{\mathbb{D}}$ and thus topological. This means the genus of the surface $X_{\mathbb{D}}$ provides a filtration of fatgraphs. In particular, a secondary structure has genus 0.

Due to the presence of the rainbow we can, w.l.o.g., collapse the backbone and maintain a key feature of RNA structures, namely, their sequence of nucleotides has a distinct 5' and 3' end and thus forms an unique oriented chain determined by the covalent bonds. In absence of twisted ribbons, there is no topological information within the backbone itself. Collapsing the backbone does of course not change the Euler characteristic since an edge and a vertex is eliminated at the same time. In order to keep track of the unpaired vertices, we attach a half-edge in the upper-half plane to the unpaired vertices. These half-edges inflate into stubs, see Fig. 2 (C).

A fatgraph can be presented algebraically by a pair of permutations (Penner *et al.*, 2010). Let $H = [2n]$ denote the set of half-edges, and σ , α and γ are three permutations over H , where each cycle in σ , α and γ presents a vertex, an edge and a boundary component, respectively. In particular, the length of cycles in σ is ≤ 2 , where the cycle of length one

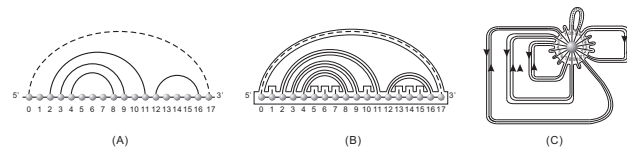


Fig. 2. (A) a secondary structure. (B) the fatgraph obtained from (A), replacing edges by ribbons and vertices by discs. The unpaired vertices are assigned a formal half-edge (stub) in the upper half-plane. (C) Collapsing the backbone into a single disc.

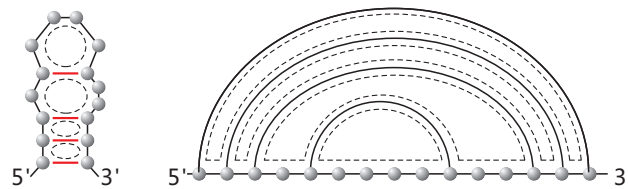


Fig. 3. Loops and their corresponding boundary components in diagram.

is evidently a bijection since α is an involution between fatgraphs having one vertex and a fatgraph having a unique boundary component. The later fatgraphs are called *unicellular maps*. The mapping is called the *Poincaré dual* and interchanges boundary components by vertices, preserving topological genus. In the following, we use π to denote the Poincaré dual.

The mapping π maps a secondary structure S into to a planar tree $T(S)$, together with the corresponding stubs, since the genus of S is zero. The underlying sequence, s , of S is by construction mapped into the boundary component of T . Let L be a T -vertex, then we denote the number of incident T -vertices by the degree of L , $\deg(L)$. In (Schmitt and Waterman, 1994) the correspondence between RNA secondary structures and (linear) trees has been constructed directly.

2.2 Topology and energy

A filtration based on the individual contributions of base pairs of RNA structures was computed via the Nussinov model (Nussinov *et al.*, 1978). (Smith and Waterman, 1978) were the first bringing energy into the picture, computing the free-energy accurately via loops. The loops—in some sense—represent the delocalization of the electrons of nearby bonds, see Fig. 3. Any fatgraph has a unique set of boundary components which determine an unique set of associated loops.

The natural concept of boundary component arising in the topological model, motivates the notion of loops, that play the key role for free energy calculations. While loops have been defined *ad hoc* for secondary structures, it is not obvious how to extend the notion to pseudoknotted configurations. This however is obtained by the following

Definition 1. Given a boundary component $\gamma = (a_1, a_2, \dots, a_n)$, let $\bar{\gamma} = (a_1, \alpha(a_2)', a_2, \dots, \alpha(a_n)', a_n, \alpha(a_1)')$, where $\alpha(a_i)' = \alpha(a_i)$ if a_i is not a α -fixed point and \emptyset , otherwise. The loop of γ is the sequence induced by $\bar{\gamma}$ by removing any \emptyset entries.

The above definition is not only compatible with respect to loops in secondary structures but also for loops in structures with pseudoknots (having higher topological genus). It is clear that we really need ribbons to arrive at this definition. This roots the loop-based energy model in



Fig. 4. Hairpin-, helix-, bulge-, interior- and multi-loops in secondary structures.

There is a distinguished loop, L_{ex} , traversing the rainbow clockwise, which is called the exterior loop.

Let σ be a sequence. To an arbitrary loop, L , we assign the energy $\eta(\sigma, L)$, where $\eta(\sigma, L_{ex}) = 0$ and $\eta(\sigma, L)$ depends on two factors: its type and the underlying backbone. Specifically this is the number of bases pairs (edges or pairs of half-edges), the number of unpaired bases (stubs) and the particular nucleotides involved. The energy of a structure S over an RNA sequence σ is then given by

$$\eta(\sigma, S) = \sum_{L \in S} \eta(\sigma, L).$$

One distinguishes for secondary structures the following three types of loops: a hairpin-, containing exactly one, an interior-, a bulge- or helix-containing two, and a multi-loop containing at least three base pairs.

Interior-, bulge- and helix-loops are differentiated by their corresponding two intervals. An interior loop having two such intervals that are non-empty, a bulge loop having one and a helix loop having none, respectively, see Fig. 4.

For a given sequence $\sigma = (y_1, y_2, \dots, y_n)$ where $y_i \in \{A, U, C, G\}$, we proceed by computing $\eta(\sigma, L)$. In the following we oftentimes write $\sigma_i = y_i$.

A hairpin, L_H is a loop having exactly one edge and one non-empty interval containing k stubs, where $k \geq 3$ due to flexibility constraints imposed by the backbone of the molecule.

In case of $3 \leq k \leq 4$ we call L a tetra-loop, which has a particular energy that depends on the two nucleotides incident to its unique edge (y_i, y_{i+k+1}) as well as the particular nucleotides corresponding to the sequence of stubs of its unique non-empty interval $(y_{i+1}, \dots, y_{i+k})$.

For any other number of stubs, k , the energy calculation depends only on k and not the particular nucleotide sequence, except of (y_i, y_{i+k+1}) and y_{i+1} and y_{i+k} . We have

$$\eta(\sigma, L_H) = \begin{cases} \eta_H((y_i, y_{i+k+1}), y_{i+1}, \dots, y_{i+k}) & \text{if } 3 \leq k \leq 4 \\ \eta_H((y_i, y_{i+k+1}), y_{i+1}, y_{i+k}, k) & \text{otherwise.} \end{cases} \quad (2)$$

An interior, bulge or helix loop, L_* , can be represented as $L_* = (e_1, s_1^1, \dots, s_{k_1}^1, e_2, s_1^2, \dots, s_{k_2}^2)$, where $e_1 = (i, \alpha(i))$ and $e_2 = (j, \alpha(j))$ are edges and $s_1^1, \dots, s_{k_1}^1, s_1^2, \dots, s_{k_2}^2$ are stubs. The energy of L_* is computed as

$$\eta(\sigma, L_*) = \begin{cases} \eta_*(y_i, y_{\alpha(i)}, y_{i+1}, y_{\alpha(i+1)}) & \text{(helix)} \\ \eta_*(y_i, y_{\alpha(i)}, y_j, y_{\alpha(j)}, y_{i+1}, y_{\alpha(i)-1}, y_{j+1}, y_{\alpha(j)-1}, k_1) & \text{(bulge)} \\ \eta_*(y_i, y_{\alpha(i)}, y_j, y_{\alpha(j)}, y_{i+1}, y_{\alpha(i)-1}, y_{j+1}, y_{\alpha(j)-1}, k_1, k_2) & \text{(interior)} \end{cases} \quad (3)$$

where $k_1, k_2 > 0$.

A multi-loop L_M contains k edges and k intervals, some of which being possibly empty, where $k \geq 3$. $\eta_M(\sigma, L_M)$ is computed by

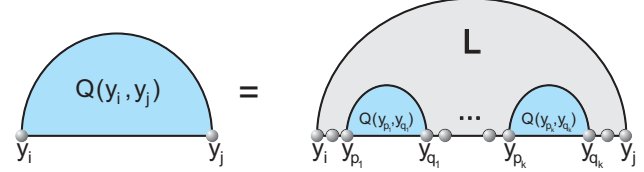


Fig. 5. The recursion for computing the partition function $Q_T(a_1, a_2)$.

2.3 The partition function

Definition 2. Let S be a secondary structure over n nucleotides. Then the partition function of s is given by

$$Q(S) = \sum_{\sigma \in \mathcal{Q}_4^n} e^{-\frac{\eta(\sigma, S)}{kT}}, \quad (5)$$

where $\eta(\sigma, S)$ is the energy of s on σ , k is the universal gas constant and T is the temperature.

In the following we recursively compute $Q(S)$. Given the structure S , we consider an arbitrary edge (i, j) , where $i <_< j$. Let $S_{i,j}$ denote the substructure of S over the interval $[i, j]$. Since S contains no crossing arcs all arcs of $s_{i,j}$ are contained in $[i, j]$, whence $S_{i,j}$ is well defined. Let

$$Q(y_i, y_j) = \sum_{\substack{\sigma \in \mathcal{Q}_4^{j-i+1} \\ \sigma|_i=y_i, \sigma|_j=y_j}} e^{-\frac{\eta(\sigma, S_{i,j})}{kT}}.$$

Since S has no crossing arcs, i is by construction the minimum half-edge of the loop containing the half-edge j , L . We remove L and suppose $(p_1, q_1) \dots, (p_k, q_k)$ are edges and d_1, \dots, d_u are stubs in L , then

$$Q(y_i, y_j) = \sum_{y_{p_i}, y_{q_i} \in \mathcal{Q}_4} e^{-\frac{\eta(\sigma, L)}{kT}} \prod_i^h Q(y_{p_i}, y_{q_i}), \quad (6)$$

We illustrate this recursion for computing the partition function in Fig. 5. The partition function $Q(S)$ is then given by $Q(0, n+1)$, where $(0, n+1)$ is the rainbow.

We remark that the routine of computing $Q(S)$ is similar to the one for finding an optimal sequence adopting to a given structure is shown in (Busch and Backofen, 2006). However, the topological model streamlines the derivations, the key here being the bijection between minimal arcs and loops.

2.4 Boltzmann sampling and patterns

Having computed the partition function $Q(S)$ as well as the $Q(y_i, y_j)$ terms puts us in position to Boltzmann sample sequences for fixed secondary structure S . Here the probability of a sequence σ to be sampled is given by

$$\mathbb{P}(\sigma) = \frac{e^{-\frac{\eta(\sigma, S)}{kT}}}{Q(S)}.$$

We build σ recursively from top to bottom, starting with the exterior loop L_{ex} . Suppose (p_t, q_t) are base pairs contained in L_{ex} and let u denote the number of unpaired bases in L_{ex} . Since $\eta(\sigma, L_{ex}) = 0$, the unpaired nucleotides in L_{ex} are sampled uniformly, i.e., with probability $1/4$. Then the probability of the event $\sigma_r = y_r$, where σ_r are nucleotides in L_{ex} , $\forall \sigma_r \in L_{ex}$, $r \neq 0, n+1$ is given by

the energy spectrum of those sequences that actually fold into S via the classic folding algorithm using the same energy functions here. The Inverse folding rate (IFR),

$$\text{IFR} = \frac{\# \text{ of sequences folding into } S}{\# \text{ of sampled sequences}}$$

measures the rate of successful refoldings from that ensemble.

Let σ be a sequence from a Boltzmann sample w.r.t. the structure S . Let \bar{S} denote the structure that σ folds to. We consider

$$\Delta(\sigma) = |\eta(\sigma, S) - \eta(\sigma, \bar{S})|$$

and compare the $\Delta G(\sigma, S)$ of several native structures contained in PDB with those of a several random structures (obtained by uniformly sampling RNA secondary structures).

The PDB structure **2JXV** (Cevec *et al.*, 2008) represents a segment of an mRNA, having length 33. The structure exhibits a tetra-loop, an interior loop and two stacks of length 8 and 5, respectively, see Fig. 8. We Boltzmann sample 10^4 sequences for this structure observing an AU ratio of 18.18%, while CG ratio is 81.82%. The IFR reads 95.16%, i.e. almost all sampled sequences refold into 2JXV. The heat map of 2JXV is given in Fig. 8 and we list the most frequent 10 patterns of the largest interval having $R_{i,j} > 0.52$ in Tab. 1 in supplement material together with their *a priori pattern* probabilities. We observe that the tetra-loop determines specific patterns. This finding is not entirely straightforward as the hairpin-loops are the last to be encountered when Boltzmann sampling. I.e. they are the most correlated loop-types in the sense that structural context influences them the most.

The energy distribution of the Boltzmann sample is presented in Fig. 9 and we observe that the inverse folding solution is not simply the one that minimizes the free energy w.r.t. 2JXV. with the best energy. $\Delta\eta(\sigma)$ -data are not displayed here in view of the high IFR.

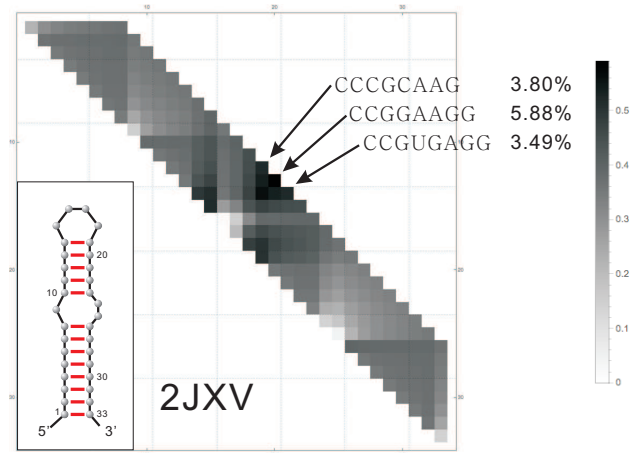


Fig. 8. The secondary structure of 2JXV and its heat-map. We display the most frequent sampled patten for the largest interval having $R_{i,j} > 0.52$. The sample size is 10^4 .

The PDB structure **2N3R** (Bonneau *et al.*, 2015) consist of 61 nucleotides and has a 3-branch multi-loop, two tetra-loops, interior loops

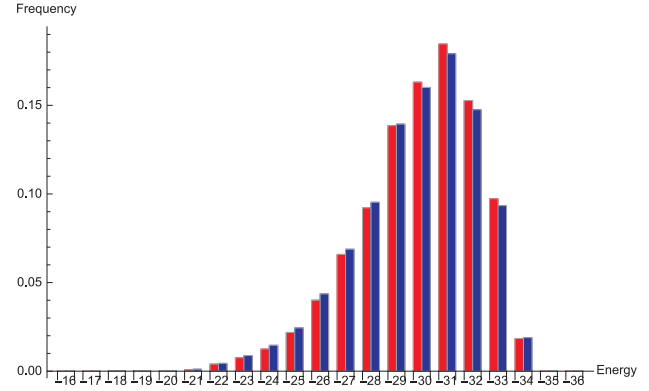


Fig. 9. The energy distribution of the Boltzmann sample for 2JXV. We display the frequency of sequences having a particular energy (blue) and the frequency of sequences that fold into 2JXV (red).

the most frequent 10 patterns in the largest interval having $R_{i,j} > 0.52$ in the Supplemental Materials, Tab. 2 together with their *a priori pattern* probabilities computed by eq. (7)

Comparing the sequence segments [17, 24] and [37, 44], both of which being tetra-loops with additional two nucleotides. The $R_{i,j}$ values of these segments are similar, approximately 0.59, however, their most frequently sampled patterns appear at different rates. For [17, 24] this pattern is CCGAAGGC and it occurs with a Boltzmann sampled frequency of 1.69% and pattern probability 1.44%, while for [37, 44] it is CGUGAGGG with sampled frequency 3.27% and pattern probability 3.24%. This makes the point that pattern frequency distributions are strongly correlated with structural context.

The energy distribution of the Boltzmann sample is given in Fig. 11 (A) and we display the $\Delta\eta(\sigma)$ -data in Fig. 11 (B) where we contrast the data with $\Delta\eta(\sigma)$ -values obtained from Boltzmann sampling 10^4 sequences of 5 random structures of the same length. We observe that the $\Delta(\sigma)$ -values for 2N3R are distinctively lower than those for random structures.

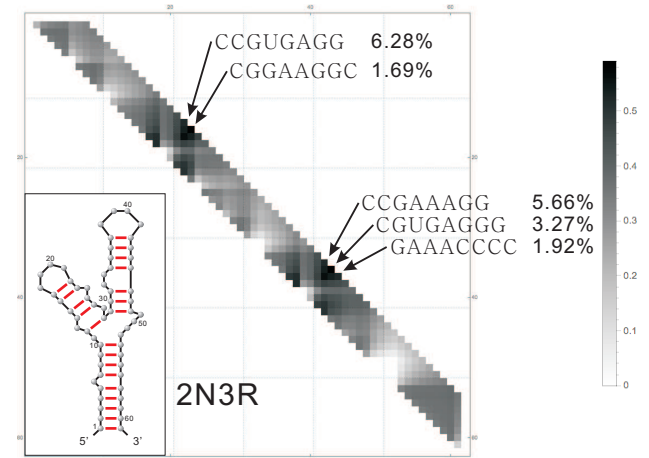


Fig. 10. The secondary structure of 2N3R and its heat map. We show the most frequent patterns for the largest interval having $R_{i,j} > 0.52$. The sample size is

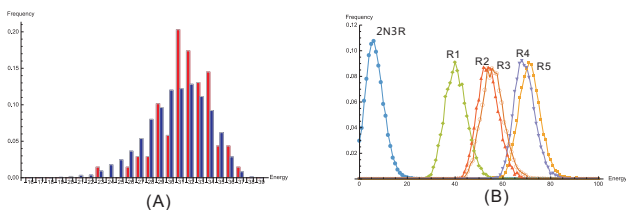


Fig. 11. (A) The energy distribution of Boltzmann sampled sequences. The frequency of sequences having a particular energy level (blue), the frequency of sequences folding into 2N3R (red). (B) $\Delta\eta(\sigma)$ -data of 2N3R versus $\Delta\eta(\sigma)$ -data of five random structures.

1EHZ in Fig. 12 The IFR is 1.3×10^{-3} w.r.t. our Boltzmann sample of size 10^4 and we display the energy distribution of the sampled sequences in Fig.13 (A). Interestingly we still find many inverse fold solutions by just Boltzmann sampling $Q(S)$ and these sequences are not concentrated at low free energy values.

In Fig. 13 (B) we display the $\Delta\eta(\sigma)$ data and contrast them with those obtained by the Boltzmann samples of five random structures. We observe a significant difference between the $\Delta\eta(\sigma)$ distribution of the 1EHZ sample and those of the random structures.

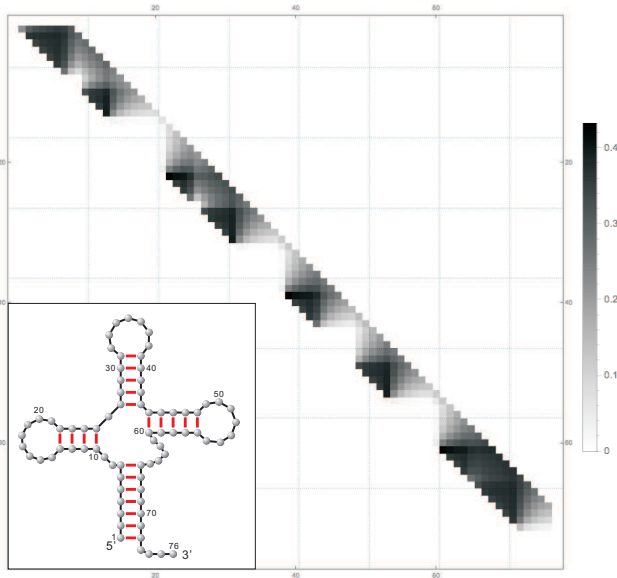


Fig. 12. The secondary structure of 1EHZ and its heat-map. We display the most frequent sampled pattern for the largest interval having $R_{i,j} > 0.52$. The sample size is 10^4 .

The three above examples indicate that sequence-structure correlations can be used to locate regions where specific embedded patterns arise. Furthermore we observe that studying $Q(\sigma)$ has direct implications for inverse folding. This is in agreement with the findings in (Busch and Backofen, 2006). Although at present we can only estimate the mutual information, we can conclude that there are sequences that cannot be aligned but obtain almost identical mutual information. This implies that sequences carry embedded patterns that cannot be

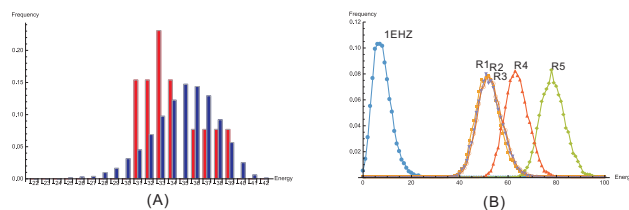


Fig. 13. (A) The energy distribution of the Boltzmann sampled sequences. The frequency of sequences having a particular energy level (blue), the frequency of sequences folding into 1EHZ (red). (B) $\Delta\eta(\sigma)$ -data of 1EHZ versus $\Delta\eta(\sigma)$ -data of five random structures.

significant context dependence on the structure. Other loops affect the energy of the hairpin loop and thus determine this particular subsequence. We observe that the embedded patterns can, for certain structures, be quite restricted, possibly elaborate and are not entirely obvious. In any case, the analysis cannot be reduced to conventional sequence alignment. The heat-maps introduced here identify the regions for which only a few select patterns appear and computed the *a priori* probabilities of their occurrence.

This type of analysis will be carried out for the far more advanced MC-model (Parisien and Major, 2008), incorporating non-canonical base pairs. This will in particular enable us to have a closer look at the hairpins of the tRNA structure. In addition we believe that this line of work may enable us to arrive at non-heuristic inverse foldings.

As mentioned above, the present analysis is just a first step and discusses embedded patterns in the sense of subsequent nucleotides. However our framework can deal with any embedded pattern. We think a deeper, conceptual analysis has to be undertaken aiming at identifying how a collection of structures provides sequence semantics. Quite possibly this can be done in the context of formal languages. We speculate that advancing this may lead to a novel class of embedded pattern recognition algorithms beyond sequence alignment.

4 Acknowledgments

Special thanks to Michael Waterman and Peter Stadler for their input on this manuscript. We gratefully acknowledge the help of Kevin Shinpaugh and the computational support team at VBI, Rebecca Wattam, Henning Mortveit, Madhav Marathe and Reza Rezazadegan for discussions.

References

- Andersen, J. E., Penner, R. C., Reidys, C. M., and Waterman, M. S. (2012). Topological classification and enumeration of RNA structures by genus. *J. Math. Biol.* preprint.
- Bon, M., Vernizzi, G., Orland, H., and Zee, A. (2008). Topological classification of RNA structures. *J. Mol. Biol.*, **379**, 900–911.
- Bonneau, E., Girard, N., Lemieux, S., and Legault, P. (2015). The NMR structure of the II-III-VI three-way junction from the neurospora VS ribozyme reveals a critical tertiary interaction and provides new insights into the global ribozyme structure. *RNA*, **21**, 1621–1632.
- Busch, A. and Backofen, R. (2006). Info-rna—a fast approach to inverse rna folding. *Bioinformatics*, **22**(15), 1823–31.
- Cevc, M., Thibaudeau, C., and Plavec, J. (2008). Solution structure of a let-7 miRNA:lin-41 mRNA complex from *C. elegans*. *Nucleic Acids Res.*, **36**, 2330–2337.

- Ding, Y. and Lawrence, C. E. (2003). A statistical sampling algorithm for RNA secondary structure prediction. *Nucleic Acids Res.*, **31**, 7280–7301.
- Do, C., Woods, D., and Batzoglou, S. (2006). Contrafold: RNA secondary structure prediction without physics-based models. *Bioinformatics*, **22**(14), e90–8.
- Eddy, S. R. (2001). Non-coding RNA genes and the modern rna world. *Nat. Rev. Genet.*, **2**(12), 919–29.
- Euler, L. (1752). Elementa doctrinae solidorum. *Novi Comm. Acad. Sci. Imp. Petropol.*, **4**, 109–140.
- Fekete, M., Hofacker, I., and Stadler, P. (2000). Prediction of RNA base pairing probabilities on massively parallel computers. *J. Comput. Biol.*, **7**, 171–182.
- Hatcher, A. (2002). *Algebraic Topology*. Cambridge University Press.
- Hofacker, I. L. (2003). The vienna RNA secondary structure server. *Nucl. Acids Res.*, **31**, 3429–3431.
- Hofacker, I. L., Fontana, W., Stadler, P. F., Bonhoeffer, L. S., Tacker, M., and Schuster, P. (1994). Fast folding and comparison of RNA secondary structures. *Monatsh. Chem.*, **125**, 167–188.
- Koonin, E. V., Gorbalenya, A. E., and Chumakov, K. M. (1989). Tentative identification of RNA-dependent RNA polymerases of dsRNA viruses and their relationship to positive strand RNA viral polymerases. *FEBS Lett.*, **252**(1-2), 42–6.
- Loebl, M. and Moffatt, I. (2008). The chromatic polynomial of fatgraphs and its categorification. *Adv. Math.*, **217**, 1558–1587.
- Massey, W. S. (1967). *Algebraic Topology: An Introduction*. Springer-Verlag, New York.
- Mathews, D., Disney, M., Childs, J., Schroeder, S., Zuker, M., and Turner, D. (2004). Incorporating chemical modification constraints into a dynamic programming algorithm for prediction of RNA secondary structure. *Proc Natl Acad Sci*, **101**, 7287–7292.
- Mathews, D. H. (2004). Using an RNA secondary structure partition function to determine confidence in base pairs predicted by free energy minimization. *RNA*, **10**(8), 1178–1190.
- McCarthy, B. J. and Holland, J. J. (1965). Denatured DNA as a direct template for in vitro protein synthesis. *Proc. Natl. Acad. Sci. USA*, **54**(3), 880–886.
- McCaskill, J. S. (1990). The equilibrium partition function and base pair binding probabilities for RNA secondary structure. *Biopolymers*, **29**, 1105–1119.
- Mount, D. M. (2004). *Bioinformatics: Sequence and Genome Analysis*. Cold Spring Harbor Laboratory Press, 2nd ed. edition.
- Nussinov, R., Piecznik, G., Griggs, J. R., and Kleitman, D. J. (1978). Algorithms for loop matching. *SIAM J. Appl. Math.*, **35**(1), 68–82.
- Orland, H. and Zee, A. (2002). RNA folding and large n matrix theory. *Nuclear Physics B*, **620**, 456–476.
- Parisien, M. and Major, F. (2008). The MC-Fold and MC-Sym pipeline infers RNA structure from sequence data. *Nature*, **452**, 51–55.
- Penner, R. C. (1988). Perturbative series and the moduli space of riemann surfaces. *J. Differential Geom.*, **27**(1), 35–53.
- Penner, R. C. (2004). Cell decomposition and compactification of Riemann’s moduli space in decorated Teichmüller theory. In N. Tongring and R. C. Penner, editors, *Woods Hole Mathematics-perspectives in math and physics*, pages 263–301. World Scientific, Singapore. arXiv: math. GT/0306190.
- Penner, R. C. and Waterman, M. S. (1993). Spaces of RNA secondary structures. *Adv. Math.*, **101**, 31–49.
- Penner, R. C., Knudsen, M., Wiuf, C., and Andersen, J. E. (2010). Fatgraph models of proteins. *Comm. Pure Appl. Math.*, **63**, 1249–1297.
- Reidys, C. M., Huang, F., Andersen, J. E., Penner, R. C., Stadler, P. F., and Nebel, M. E. (2011). Topology and prediction of RNA pseudoknots. *Bioinformatics*, **27**, 1076–1085.
- Schmitt, W. and Waterman, M. (1994). Linear trees and rna secondary structure. *Disc. Appl. Math.*, **51**, 317–323.
- Schuster, P. (1997). Genotypes with phenotypes: adventures in an RNA toy world. *Biophys. Chem.*, **66**(2-3), 75–110.
- Schuster, P., Fontana, W., Stadler, P. F., and Hofacker, I. L. (1994). From sequences to shapes and back: a case study in RNA secondary structures. *Proc Biol Sci.*, **255**(1344), 279–84.
- Shi, H. and Moore, P. B. (2000). The crystal structure of yeast phenylalanine tRNA at 1.93 Å resolution: a classic structure revisited. *RNA*, **6**, 1091–1105.
- Smith, T. and Waterman, M. (1978). RNA secondary structure. *Math. Biol.*, **42**, 31–49.
- Temin, H. and Mizutani, S. (1970). RNA-dependent DNA polymerase in virions of rous sarcoma virus. *Nature*, **226**(5252), 1211–3.
- The 1000 Genomes Project Consortium (2015). A global reference for human genetic variation. *Nature*, **526**(68-74).
- Uzawa, T., Yamagishi, A., and Oshima, T. (2002). Polypeptide synthesis directed by DNA as a messenger in cell-free polypeptide synthesis by extreme thermophiles, thermus thermophilus HB27 and sulfolobus tokodaii strain 7. *J. Biochem*, **131**(6), 849–53.
- Waterman, M. S. (1978). Secondary structure of single-stranded nucleic acids. *Adv. Math. (Suppl. Studies)*, **1**, 167–212.
- Zuker, M. and Stiegler, P. (1981). Optimal computer folding of larger RNA sequences using thermodynamics and auxiliary information. *Nucleic Acids Res.*, **9**, 133–148.

SUPPLEMENTARY MATERIAL OF
SEQUENCE-STRUCTURE RELATIONS OF BIOPOLYMERS

[12, 19] : 0.52			[13, 20] : 0.59			[14, 21] : 0.52		
Patten	Fr (%)	Pb (%)	Patten	Fr (%)	Pb (%)	Patten	Fr (%)	Pb (%)
CCCGAAAG	3.80%	3.45%	CCGGAAGG	5.88%	5.74%	CGCAAGGG	3.49%	3.51%
CCCGCAAG	3.47%	3.45%	CCGUGAGG	5.87%	5.74%	CGUGAGGG	3.49%	3.51%
CCCGGAAG	3.33%	3.45%	CCGCAAGG	5.82%	5.74%	CGAAAGGG	3.29%	3.51%
CCCGUGAG	3.31%	3.45%	CCGAAAGG	5.67%	5.74%	CGGAAGGG	3.26%	3.51%
GGGGAGAC	2.56%	2.40%	GGGGGACC	3.97%	3.74%	GGAGACCC	2.40%	2.35%
GGGGAAAC	2.56%	2.40%	GGGAAACC	3.81%	3.74%	GGGGACCC	2.39%	2.35%
GGGGGGAC	2.35%	2.40%	GGGUGACC	3.76%	3.74%	GGAAACCC	2.36%	2.35%
GGGGUGAC	2.35%	2.40%	GGGAGACC	3.58%	3.74%	CUUCGGGG	2.18%	1.84%
GCCGUGAG	2.16%	2.03%	GCGUGAGC	3.35%	3.18%	CGCAAGCC	2.12%	1.99%
GGCGAAAG	2.09%	2.04%	GCGCAAGC	3.33%	3.18%	CGCAAGGC	2.10%	2.02%

TABLE 1. PDB: 2JXV. We list the most frequent (Fr) 10 patterns of the largest interval having $R_{i,j} > 0.52$ as well as their *a priori pattern* probabilities (Pr).

[16, 23] : 0.52			[17, 24] : 0.59			[36, 43] : 0.52		
Patten	Fr (%)	Pb (%)	Patten	Fr (%)	Pb (%)	Patten	Fr (%)	Pb (%)
CCGUGAGG	6.28%	5.69%	CGGAAGGC	1.69%	1.44%	CCGAAAGG	5.66%	5.62%
CCGCAAGG	5.79%	5.69%	CGCAAGGU	1.67%	1.44%	CCGUGAGG	5.63%	5.62%
CCGGAAGG	5.63%	5.69%	CGGAAGGG	1.67%	1.44%	CCGCAAGG	5.45%	5.62%
CCGAAAGG	5.39%	5.69%	CGUGAGGG	1.62%	1.44%	CCGGAAGG	5.34%	5.62%
GGGGGACC	4.02%	3.78%	CGCAAGGG	1.53%	1.44%	GGGGGACC	4.02%	3.83%
GGGAGACC	3.75%	3.78%	CGAAAGGC	1.52%	1.44%	GGGAAACC	4.01%	3.83%
GGGAAACC	3.56%	3.78%	CGUGAGGU	1.50%	1.44%	GGGUGACC	3.79%	3.83%
GCGAAAGC	3.48%	3.21%	CGAAAGGU	1.48%	1.44%	GGGAGACC	3.72%	3.83%
GGGUGACC	3.42%	3.78%	CGAAAGGG	1.47%	1.44%	GCGCAAGC	3.57%	3.26%
GCGGAAGC	3.39%	3.21%	CGGAAGGA	1.44%	1.44%	GCGGAAGC	3.51%	3.26%
			[37, 44] : 0.59			[38, 45] : 0.52%		
			Patten	Fr (%)	Pb (%)	Patten	Fr (%)	Pb (%)
			CGUGAGGG	3.27%	3.24%	GAAACCCC	1.92%	1.76%
			CGCAAGGG	3.21%	3.24%	GGGACCCC	1.76%	1.76%
			CGAAAGGG	3.15%	3.24%	GGAAGGGC	1.68%	1.53%
			CGGAAGGG	2.92%	3.24%	GAAAGGCC	1.67%	1.52%
			GGUGACCC	2.47%	2.54%	GUGACCCC	1.63%	1.76%
			GGAGACCC	2.46%	2.54%	GAGACCCC	1.63%	1.76%
			CGGAAGCC	2.38%	2.16%	GAAAGGGC	1.60%	1.53%
			GGAAACCC	2.36%	2.54%	GUGAGGCC	1.57%	1.52%
			CGUGAGGC	2.34%	2.19%	GCAAGGCC	1.56%	1.52%
			GGGGACCC	2.33%	2.54%	GGAAGGCC	1.51%	1.52%

TABLE 2. PDB: 2N3R. We list the most frequent (Fr) 10 patterns of the largest interval having $R_{i,j} > 0.52$ as well as their *a priori pattern* probabilities (Pr).